Analyst

A microfluidic microparticle-labeled impedance sensor array for enhancing immunoassay sensitivity

Journal:	*Analyst*
Manuscript ID	AN-ART-10-2020-002081.R2
Article Type:	Paper
Date Submitted by the Author:	08-Mar-2021
Complete List of Authors:	Khodayari Bavil, Ali; Texas Tech University, Mechanical Engineering Sticker, Drago; Kobenhavns Universitet, Department of Pharmacy Rothbauer, Mario; Technische Universitat Wien, Faculty of Technical Chemistry; Medical University of Vienna, Department of Orthopedics and Trauma Surgery - KCLOB Ertl, Peter; Vienna University of Technology, Faculty of Technical Chemistry Kim, Jungkyu; University of Utah, Mechanical Engineering

A microfluidic microparticle-labeled impedance sensor array for enhancing immunoassay sensitivity

Ali Khodayari Bavil[1,2] (https://orcid.org/0000-0002-9717-9136)

Drago Sticker[3] (https://orcid.org/0000-0001-7688-6977)

Mario Rothbauer[3] (https://orcid.org/0000-0002-9928-3631)

Peter Ertl[3], (https://orcid.org/0000-0002-7625-2445)

Jungkyu Kim[1,2]* (https://orcid.org/0000-0003-3691-6953)

[1] *Department of Mechanical Engineering, University of Utah, Salt Lake City, UT*

[2] *Department of Mechanical Engineering, Texas Tech University, Lubbock, TX*

[3] *Faculty of Technical Chemistry, Vienna University of Technology, Vienna, Austria*

* Address correspondence to Jungkyu (Jay) Kim

Department of Mechanical Engineering

University of Utah

Salt Lake City, Utah 84112, USA

Phone: (801) 581-6743

E-mail: jkim@mech.utah.edu

Abstract

An impedimetric biosensor is used to measure electrical impedance changes in the presence of biomolecules from sinusoidal input voltages. In this paper, we present a new portable impedance-based biosensor platform to improve the sensitivity of immunoassays with microparticles as a label. Using a 2×4 interdigitated electrode array with a 10/10 μm electrode/gap and a miniaturized impedance analyzer, we performed immunoassays with microparticles by integrating a microfluidic channel to evaluate signal enhancement. First, to understand the material dependency of microparticles on the sensor array, magnetic, silica, and polystyrene microparticles were tested. Among these microparticles, magnetic microparticles presented high signal enhancement with relevant stability from the sensor array. With the magnetic microparticles, we demonstrate a series of immunoassays to detect human tumor necrosis factor (TNF-α) and compare the level of signal enhancement by measuring the Limit of Detection (LOD). With the microparticles, we achieved over ten times improvement of LOD from sandwich immunoassays. By incorporating with sample preparation and flow manipulation systems, this impedance sensor array can be utilized for digital diagnostics for a real sample-in answer-out system.

Keywords: Interdigitated electrode array, microparticles, hydrodynamic force, digital immunoassay, microfluidics, sensitivity enhancement

Introduction

An impedimetric biosensor is a class of electrochemical biosensors that measures electrical impedance change due to the presence of biomolecules[1], cells [2], or labeled biomaterials[3] on a working electrode by applying a sinusoidal voltage. This sensor has shown a promise for digitalized point-of-care diagnostics (POC) due to low-cost, ease of miniaturization, multiplexing ability, and label-free operation[4, 5]. To date, much effort has been made in conjunction with developing a miniaturized platform with reduced complexity. Ha et al. developed an integrated cell-counting assay system for malaria diagnosis consisting of a microfluidic chip and a small impedance circuit board[6]. Another integrated diagnostic platform was proposed to detect transgenic protein Cry1Ab consisted of a printed gold electrode chip and a microfluidic flow cell[7]. For miniaturized and portable impedimetric biosensor platform, an impedimetric reader based on the AD5933 chip was designed with a microfluidic channel on IDE array for Deep Vein Thrombosis and pulmonary embolism diagnosis[4]. Although much effort has been done on developing a miniaturized impedance biosensor, an easy-to-use and integrated platform with sufficient sensitivity to conduct real immunoassays is poorly developed.

To improve the sensitivity of impedimetric biosensors, several design parameters have been considered. Typically, an interdigitated electrode (IDE) is used for impedimetric biosensors because they have the advantages of high signal-to-noise ratio, low ohmic drop, and fast attainment of steady-state[8, 9]. Critical parameters of an IDE design are the sensing area, electrode gap, and frequency range. The design of the IDE array[10, 11] itself can increase the overall sensitivity of IDEs due to considerations of the overall sensing area[12]. Electrode gap is the most significant parameter on the sensitivity of IDE biosensors since the electric field between two electrodes can effectively be changed during biomolecular binding events. The sensitivity will further increase when the distance between the two electrodes decreases from micro-gap into nano-gaps[13-15]. As the distance between electrodes becomes smaller, the chances of short-circuiting of the electrodes by the sample as well as labels increase, which can result in failed measurements. It should be also noticed that nano-gaps will require a buffer solution with a very low ionic strength to maintain a proper baseline, which can affect the antigen-antibody interaction[16]. Additionally, nano-gap IDE requires complex fabrication procedures, resulting in higher manufacturing costs, lower yield rate, and lower practicality. Therefore, the typical gap between the electrode fingers for biosensing

platforms is suggested to be 1-10 μm[17]. The selection of an appropriate frequency is another key parameter associated with assay sensitivity[18]. At lower frequencies (< 1 kHz), the impedance is dominated by the leakage resistance of the IDEs, which is highly sensitive to the electrode material[19]. For high frequencies above 100 kHz, solution resistance contributes to the net impedance, and measurement errors increase from parasitic capacitances and inductances. In the mid frequencies (1 kHz ~ 100 kHz), the measurement signals rely on the electrode surface capacitance allowing the affinity binding on the IDEs to be detected[20]. Therefore, most impedimetric biosensors adopt a frequency between 1 kHz to 100 kHz, commonly around 10 kHz, where the signal is relatively stable, and the impedance response is dominated by the interfacial changes[10, 20-22].

In addition to these design parameters, the overall sensitivity of impedimetric biosensors can also be improved by using micro- or nano-particles as a label to amplify impedance signals by inducing interfacial changes[23-26]. Although labeling with particles in electrochemical biosensors has been widely used, it should be noted that the data recording under PBS is better since electrochemical buffers being used for faradic measurements usually act as a mild oxidant that can denature some proteins[27]. Additionally, microparticle-labeling in non-faradaic (or capacitive) biosensors are inherently simpler and more amenable for POC testing with the ability to make measurements related to the change in interfacial capacitance during the affinity binding, without redox reaction to be completed as is required in faradic biosensors[17]. There are two distinct approaches to improve overall immunoassay performance. By coating gold nanoparticles on a IDE electrode electrochemically, overall surface area of the electrodes increased significantly so that signal-to-noise ratio was promoted to detect TNF-α[26]. Even though this work showed proper improvement on sensitivity, the extensive surface preparation for IDE and biofunctionalization and further fabrication steps limit to be more compelling POC platforms. Another approach is to use micro/nanoparticles to improve overall sensitivity. Several studies have demonstrated the effects of particle size and material on the sensitivity[28, 29]. From theoretical analysis, labeling particles can effectively block the electric fringing fields, resulting in an increment of impedance with respect to the width and gap of the IDEs[9, 30]. With this principle, a sandwich immunoassay for quantifying carcinoembryonic antigen was conducted using gold nanoparticles (GNP), and a detection limit of 1 ng/mL was achieved[31]. Similarly, a real-time impedance-based immunosensor conjugating Galectin-1 antibodies to alumina nanoparticles was used to improve sensitivity and

immobilization efficiency for quantifying of Galectin-1 protein[22]. Even though labeling with these particles has been utilized in various assays to improve the sensitivity, overall achievements are insignificant due to a lack of understanding of the effect of these particles, comparison of the signal enhancement with labeling, and implementing proper immunoassay procedures.

A typical microparticle based assay requires a microfluidic channel to induce controllable hydrodynamic forces [32-34]. It is found that hydrodynamic forces between 0.1 and 10 pN can rupture non-specific bonds and that those between 6 and 250 pN preserve specific bonds[35-37]. Therefore, exploiting the controlled hydrodynamic washing forces imposed by the flow velocity in the microfluidic channel is critical to knock down non-specifically bound microparticles from the IDE array, improving the overall signal to noise ratio[38].

With these concepts using microparticle-based signal enhancement and a microfluidic system, we developed a miniaturized impedimetric biosensor including all necessary components for bioassays within a single platform, which consists of a gold IDE array chip for multiplexed assays, a small custom-made 8-channel impedance analyzer connected to a semi-real time data acquisition software, and a PDMS microfluidic channel for sample delivery and hydrodynamic washing purpose (see **Figure S1**). To further improve the sensitivity of the immunoassay, we incorporated a microparticle labeling method. First, we tested three different types of microparticles at a fixed size to figure out the effect of material property and surface charges on the readout sensitivity. From these preliminary tests, magnetic microparticles showed optimal performance and were then utilized as labeling for human tumor necrosis factor-alpha (TNF-α) immunoassay. Anti-human TNF-α was covalently bonded onto the IDE surface through EDC/s-NHS mediated bioconjugation. Then different concentrations of the target analytes and anti-TNF-α antibodies conjugated with magnetic microparticles were introduced as a detector. By obtaining immunosensor responses (normalized impedance variation) from surface coverage of microparticles settling on IDE electrodes, the limit of detection (LOD) was improved from 0.99 ng/mL for label-free detection to 83 pg/mL for microparticle-labeling bioassay.

Materials and Methods

Design of the Impedance Sensing Platform

Impedance based immunosensors utilize the formation of immunocomplex (e.g., antibody as a bioreceptor and specific antigen as its corresponding analyte) in a thin film configuration on the electrode surface. This complex formation alters the interfacial capacitance and resistance at the electrode/electrolyte interface. The electrical impedance signal is expressed as the ratio of the voltage phasor to the electric current phasor. The discrepancy between these two phasors occurs when electric fields on the sensing electrode are disrupted or/and altered by the presence of biomolecules at the electrode interface. Here, a custom-made microfluidic impedance measurement system is designed, as shown in **Figure 1,** consisting of a gold (Au) IDE array chip, an impedance analyzing circuit, a data acquisition (DAQ) board associated with a LabVIEW software, and a microfluidic channel. The Au IDE array chip having a finger width and spacing of 10 μm was fabricated on a glass wafer based on a conventional photolithography process and Ti/Au deposition to realize eight sets of IDEs on a square glass chip (30 × 30 mm). Electric impedance in the analyzer circuit is measured by a 12-bit impedance converter chip, AD 5933 (Analog Devices Inc.). A detailed sketch of the setup is illustrated in **Figure S1**. Sinusoidal excitation signal (V_{PP} = 200 mV) is applied to each pair of IDEs, and the circuit board reads the resulting current and calculates the Discrete Fourier Transform (DFT). Since DFT measures the frequency-dependent energy of signals, the magnitude and phase of impedance Z at the frequency can be obtained by the following equations:

$$Z = \frac{v_i}{i_0} = \left|\frac{V_i}{I_o}\right| \angle \varphi_i - \varphi_o = \left|\frac{V_i R_{fb} R_A}{V_o}\right| \angle -\varphi_o \qquad (1)$$

, where v_i, i_o, V_i, I_o, φ_i, φ_o, R_{fb}, R_A, V_o are sinusoidal input voltage, output current, input voltage magnitude, output current magnitude, phase of the input signal, phase of the output signal, feedback resistance, internal amplifier gain, output voltage magnitude, respectively. The AD5933 stores the real (R) and imaginary (I) values of DFT at two 16-bit registers. The two data registers are accessed by the DAQ board using I2C protocol and saved in the customized LabVIEW software after data processing. The gain factor and system phase offset were first calibrated by measuring a resistor of known impedance with an LCR-Meter (VSP/VMP3, Bio-Logic Science Instruments) swiping the frequency in the preferred range of 11kHz to 91kHz. (**See Figure S5**)

Equivalent Circuit of Microparticle-Amplified Impedance Sensor

Since the proposed IDE biosensor is considered as a non-faradic with microparticle amplification, to a better understanding of its working principle, an equivalent circuit model of a two-electrode system can be investigated. The sketch of this equivalent circuit is shown in **Figure S2.** C_g is the geometric capacitance of the electrodes determined by the dimensions of the electrodes (thickness, gap, etc.) and the dielectric of the surrounding solution. C_{dl} denotes the double-layer capacitances of the two electrodes and appears at the interface between a conductive electrode and an adjacent buffer solution. At this boundary, two ionic layers with opposing polarities on the electrode surface and buffer are formed when a voltage is applied. The two layers of ions are separated by a single layer of solvent molecules, adhering to the surface of the electrode and acts as a dielectric in a conventional capacitor. R_s is the resistance of the buffer solution between the two electrodes that changes based on the buffer solution and not affected by the interfacial affinity. R_s is dependent on the space filled by the buffer and therefore depend on the length of the electrodes and the size of the gap between them[39]. To validate each of these components, the simplified Randles equivalent circuit was simulated using Simulink, MATLAB (**Figure S4**).

Considering the immobilization procedure for capture antibody, they are most likely to be immobilized between the electrodes since oxygen plasma treatment generates hydroxyl groups on the glass surface. Therefore, by conducting microparticle-amplified IDE immunoassay, the microparticles are located mostly in between the electrodes. In this case, the microparticles affect the impedance between electrodes, introducing their resistivity, and double-layer capacitances to the gaps [40]. The part highlighted in **Figure S2** as the "microparticle effect" is the equivalent component induced by a single microparticle. For high target concentrations, multiple microparticles will locate between the electrodes, and the corresponding equivalent component will be repeated in series resulting in changes for impedance measurements.

Microfluidic Integration

For a simple microfluidic integration, a PDMS-based microfluidic channel was fabricated by soft lithography as explained in our previous study[34]. The height and width of the channel were 110 μm and 2.5 mm, respectively, which is enough to cover the entire area of IDEs. Sample solutions were applied using a pipette from an inlet of the microfluidic channel, and a mini-vacuum

pump (12/02EB, Thomas Pump) was placed in the outlet to drive all solutions for immunoassays as well as performing hydrodynamic washing to remove unbound microparticles.

Characterization of Microparticles

To evaluate the amplification effect of various material microparticles on impedance signals, magnetic (Dynabeads M-280, Thermofisher Scientific, USA), polystyrene (08-19-303, Micromod, Germany), and silica (43-19-303, Micromod, Germany) microparticles covered by streptavidin (SA) were selected. At first, to estimate the effect of material on the impedance signal, these three different microparticles with 2.8 μm were investigated using impedance spectroscopy at 5% IDE surface coverage. To control the percentage of surface coverage by microparticles, we diluted the microparticle suspension and measured the surface coverage under the microscope after they sedimented on the surface (30seconds). Then, these microparticles were boiled at 120 ℃ for 120 minutes to denature all proteins on the surface to decouple the effect of surface charges from the material variations. From these measurements, we determine an optimal microparticle for following a series of immunoassays. In addition, the resolution of the IDE sensing platform was verified by measuring impedance with respect to the surface coverage of magnetic microparticles. After preparing various microparticle coverages (0.01~10%) on the IDE array, the impedance magnitude changes were measured to estimate the overall LOD of this platform.

Surface Functionalization and on-chip human TNF-α Immunoassay

For demonstrating immunoassay using an impedance sensor, the IDE surface was functionalized with a capture antibody (Anti-TNF-α, Abcam, UK) as a receptor to detect TNF-α. In this study, carbodiimide induced cross-linking was utilized to immobilize the capture antibody on the glass surface of the Au electrode spacing. **Figure S6** depicts the whole process of surface functionalization and immuno-conjugation. The IDE chip was first cleaned by treating with freshly prepared piranha solution (H_2SO_4/H_2O_2 3:1 V/V) for 30 seconds, followed by extensive rinsing with deionized (DI) water and dried with nitrogen. The patterned PDMS film (HT 6240 Rogers Corp., USA) with opening windows on the IDE arrays was then placed on the cleaned IDE chip to apply biochemistry reaction only on the sensing area. After treating with oxygen plasma, the hydroxylated sensor surface was functionalized with 3 % (3-Aminopropyl) triethoxysilane (APTES) to obtain an amine-functionalized surface. To adapt the carbodiimide coupling method, capture antibodies were activated by1-Ethyl-3-(3-dimethylaminopropyl) carbodiimide (EDC) and

Sulfo N-hydroxysuccinimide (Sulfo-NHS) (Thermo Scientific, USA), and then coupled with APTES-modified surface. After incubating the capture antibodies with the cross-linking reagents for 40 minutes, the IDE chip was rinsed with DI water. Then human TNF-α (ab9642, Abcam, USA) as target analyte with seven different concentrations (10 μg/mL ~100 pg/mL with 10-fold dilution) was further incubated on the patterned regions for 30 minutes. Afterward, the PDMS microfluidic device was attached to the glass slide via oxygen plasma treatment. Diluted Phosphate Buffer Saline (PBS) with 1% W/V bovine serum albumin (BSA) (1% PBSB) solution was first injected through a microchannel and incubated for 30 minutes for surface passivation. Then, biotinylated anti-human TNF-α antibodies (R&D Systems, USA) are conjugated with SA-coated microparticles, and the microparticles were introduced into the microchannel using an external mini-pump. We measured impedance signal in every single step of forming immunocomplex layers, and before each measurement, washing was carefully conducted with the proper buffer solution to thoroughly remove unbound molecules and ion residues. To eliminate the effects of variation in the baseline values, we normalized the impedance response during the measurements (ΔZ) with the initial impedance to each pair of IDEs (Z_0), and this is referred to as the normalized impedance variation ($\Delta Z/Z_0$).

Results and Discussion

Influence of Buffer Concentration on Impedance Sensor Performance

An appropriate buffer should be selected for an optimal microparticle-labeled impedance sensing since impedance sensors are highly sensitive to buffer solutions. First, the impedance values were measured from our impedance analyzer, the simulated Randles model, and validated with the LCR meter for various PBS concentrations. **Figure 2** shows all measurements and simulation results over the examined frequencies of 11 kHz to 91 kHz for PBS concentrations of 1 mM~0.001 mM, demonstrating similar trends and consistent results for all obtained values. From detailed comparison studies with the simulation result for 0.001 mM PBS at 11 kHz, we observed 11% and 13.5% differences from the LCR meter and our portable impedance analyzer, respectively . These differences under the low buffer concentration can be originated from manufacturing variations of the IDE electrodes since the impedance signals are more sensitive to the electrodes at lower frequency[19]. For this work, we mainly used normalized impedance variations for immunoreaction, so this much differences can have minimal impact on the measurements. As shown in **Figure 2**, PBS buffers with concentrations of 0.1 mM and above show similar impedance magnitude at the range of < 5 kΩ, where the signal is dominated by the buffer solution. By further diluting of PBS to 0.01 mM, the impedance magnitudes increase into the range of >10 kΩ. Since impedance variations from immunoreactions cannot be differentiated under highly conductive and saturated buffer solutions, 0.01 mM PBS or lower PBS concentrations are suitable for impedance-based immunoassays. However, if PBS concentration is too low, the buffering capacity is dwindled[41]. By considering the background signal and buffering capacity, 0.01 mM PBS was selected as a sample buffer solution for all subsequent experiments.

Microparticle Material Composition on Impedance Sensor Performance

Since the material and surface characteristics of microparticles have a significant impact on the impedance signals, we investigated the effect of various microparticles on impedance measurements. Generally, microparticles affect the capacitance by forming dielectric layers as well as the resistance by blocking the electric field fringe[10], as can be predicted from the equivalent circuit (Fig S2). **Figure 3** shows normalized impedance variation induced by various

microparticles over the frequency range of 11kHz to 91kHz, representing both values of resistance and capacitance ($Z = Z_R + Z_c = R + \frac{1}{j\omega C}$). Here, the impedance values are normalized with respect to the baseline signal from the buffer solution for each IDE. To decouple the effects of materials and surface of the microparticles, SA coated microparticles and denatured microparticles are prepared for these characterization experiments. For polystyrene and silica microparticles with SA, the impedance variation percentage changes with respect to the frequency from 1.10% to 3.04% and 1.11% to 2.02%, respectively. After denaturing these microparticles, the impedance variations increase to 3.98~4.53% for polystyrene and 4.08~4.85% for silica. However, for the magnetic particles, we observed that the impedance variations decrease to 2.16~3.36% for denatured microparticles. These results can be explained by the interfacial interaction in the presence of SA on the microparticles and promoting microparticle surface charge. For silica and polystyrene microparticles, the surface charges bridge the electric field and contribute to lower impedance variation compared with the denatured condition. Whereas the absence of surface charges in electrically permeable superparamagnetic microparticles increases permittivity and the overall impedance variations slightly drop. It is also observed that normalized impedance variations for electrically impermeable materials decreases by ascending of the measuring frequency, revealing that for both SA-coated and denatured conditions, capacitance effects are more dominant rather than resistance. However, the impedance variations for magnetic microparticle are less dependent on the applied frequency, demonstrating that the resistance formed by magnetic microparticles is more dominant than the double-layer capacitance imposed by non-conductive particles (see **Figure S2**). For the magnetic microparticles, polarization effects are also contributed to the overall impedance magnitude that has been widely discussed in our previous study for Hall-effect biosensors[42-44]. When magnetic microparticles locate in between the IDEs, the external electric field polarizes magnetic microparticles and, therefore, alters the evenly distributed electric field in the vicinity of the microparticles resulting in higher resistance[45]. Additionally, by calculating the relative standard deviation (RSD%), the normalized impedance variation demonstrated better precision for magnetic microparticles (11%) compared to the polystyrene (21%) and silica (19%) in the studied frequency range of 11kHz to 91kHz. Based on the above-mentioned considerations, magnetic microparticles were selected for the consequent measurements due to their higher output signal and better precision.

Influence of Surface Functionalization of Impedance Variations

The normalized impedance variations after surface functionalization are depicted in **Figure 4**. APTES is the first layer on top of the bare electrode, and an immobilized capture antibody is the second layer. Although the single-layer thickness of APTES is assumed to be less than 10 nm[46], its coverage as the first capacitance layer results in significant impedance increments. This well agreed with the literature, demonstrating the importance of the first layer, suggesting to minimize its capacitance as much as possible to improve the sensitivity during immunoassay[47]. After adding the capture antibody, the normalized impedance variation increased due to the antibody layer. From these thickness variations, 11 kHz shows the most responsive frequency by electrical-double layer capacitance compared with other frequencies[21], so we selected 11 kHz for further measurements.

Hydrodynamic washing for effective immunoassays

As discussed in our previous study[34], to ensure that a microparticle-labeled immunoassay is highly sensitive, the surface of the substrate should be washed with a hydrodynamic force sufficient to remove unspecific microparticles. After introducing the detection antibodies conjugated with microparticles, the washing step was conducted in the microfluidic channel. We kept the buffer volumetric flow rate constant at 20 μL/min by applying a negative pressure in the microchannel outlet using the small mini pump. This volumetric flow rate corresponds to an average velocity of 1.3 mm/s in the channel generating a total force of 40 pN on the microparticles. The total forces are less than the adhesion strength in the immunocomplex; however, they are sufficient to dislodge non-specific bindings from the surface[34, 37].

On-chip Human TNF-α Immunoassay

Human TNF-α immunoassay was conducted on the proposed impedance-based biosensor. TNF-α has important pro-inflammatory properties, which play crucial roles in the innate and adaptive immunity, cell proliferation, and apoptotic processes. Increased concentrations of TNF-α are found in acute and chronic inflammatory conditions (e.g., trauma, sepsis, infection, arthritis)[48, 49]. The human TNF-α contains 157 amino acids with a molecule weight of 17.4 kDa and an isoelectric point (pI) of 5.8[49].

To conduct the immunoassay, human TNF-α with seven different concentrations (10 μg/mL to 100 pg/mL) was first incubated on capture antibody-modified IDEs for label-free detection. After measuring the impedance signals, the anti-TNF-α conjugated magnetic microparticles were added to conduct a sandwich immunoassay to investigate signal enhancement. **Figure 5A** shows the distribution of the microparticles associated with the different concentrations of TNF-α. From surface coverage images, we could observe that microparticle coverages are proportional to the concentration of target biomolecules. By obtaining a series of impedance variations adjusted by a background signal, we found that these differential magnitudes increase due to the increasing number of microparticles, as shown in **Figure S7**. From LOD calculation at 11 kHz, this sensor can detect as low as 0.1 % change of surface coverage of magnetic microparticles. Further measurements have been performed with the impedance analyzer. **Figure 5B** shows the standard curves, representing the relation between the relative impedance signal and the analyte concentration for the label-free and microparticle-labeled immunoassays. From statistical analyses, the limit of detection (LOD) of 0.9 ng/mL and 83.46 pg/mL have been achieved for label-free and microparticle-labeled immunoassays, respectively (See Eq. S5)[50, 51]. The microparticles enable one order of magnitude improvement in LOD. In the case of the label-free assay, TNF-α molecules bind to the capture antibody and contribute an additional capacitance layer by forming a thin TNF-α molecular layer. Since the pI of TNF-α is 5.8, it has partially negative charges in the PBS buffer with a pH of 7.4. As the concentration of TNF-α antigen is increased, more negative charges are accumulated in between the electrodes, resulting in higher electric field dispersion and impedance variation[52]. When labeling with magnetic microparticles, higher impedance variation is observed compared to the label-free assay due to the blockage of the electric field and material properties of the microparticles. For higher concentrations of the target, magnetic microparticles become closer to each other and may locate on the electrodes even though they are expected to be immobilized in between the electrodes on the functionalized area of glass. In this case, the polarized microparticles between the IDEs under the electric field generate an additional magnetic field, especially when the distance is smaller than the Debye lengths[43, 45]. This results in a high impedance variation signal for higher concentrations of the target (>100 ng/mL). However, it also increases the SD due to the variation of microparticle distances from each other as well as random polarization[53]. Additionally, to quantify the precision of the assays, coefficient of variations (CV) were investigated. In this work, we achieved CV below 20% from both label-

free and microparticle labeled assays, which is an appropriate CV over the dynamic range of the target biomolecule concentration[54].

Table 1 introduces non-faradic IDE-based immunosensors for various targets and interfaces. Generally, label-free detection shows less sensitivity compared to those employing signal enhancement techniques. Although the sensitivity of some label-free immunosensors have been improved by optimizing the detection protocol and finger geometry of IDEs[55], signal enhancement techniques show more promising and cost-effective results for improvement of the overall LOD. Given more than one order of magnitude in overall LOD with microparticle labeling method and controlled hydrodynamic washing force through a microfluidic channel in this study, the impedance signal can be further enhanced if the signal enhancement technique is supplemented with optimized IDE spacing characteristics.

Table 1: Comparison between analytical parameters from IDE-based immunosensor

Target biomolecule	**LOD [ng/mL]**	**Electrode spacing**	**Microfluidic component**	**Time**		**Remark**	**Ref.**
				Functionalization /Preparation	**Assay [min]**		
Human Serum Albumin	200	4-20 µm	No	>135	60	Label-free	[56]
Cardiac troponin I	0.2	-	No	>12h	120	Label-free Surface area enhanced by GNP	[27]
Plasmodium lactate dehydrogenase	0.25	8 µm	No	>12h	120	Label-free	[55]
Carcinoembryonic antigen (CEA)	1	20 µm	No	>44h	30	Impedance signal enhanced by GNP Single electrode utilized	[31]
TNF- α	0.083	10 µm	Yes	<2h	30	Magnetic microparticle for signal enhancement	Present

Conclusion and Perspective

By developing various biosensors for detecting biomolecules, enhancing the sensitivity of these platforms has drawn lots of attention. In this study, we successfully developed an impedimetric biosensor consisting of a small impedance analyzer, a data acquisition board, and an IDE array integrated with a microfluidic channel. The impedance signal from this platform was first verified by simulation in MATLAB Simulink and an LCR meter. The resolution of the platform to detect a single layer of biomolecule and microparticle detection was examined, and a real assay was conducted to quantify the human TNF-α. After testing three different types of the microparticle, the detector antibodies were labeled with that of generating the highest and consistent impedance signal. We could improve the LOD by order of magnitude compared to the label-free bioassay using magnetic microparticles. This novel, sensitive impedance biosensor with a microparticle-labeling method for signal enhancement utilizes microfluidics for controlled hydrodynamic washing forces that has potential for POC application.

Among various digitized biosensors, impedimetric biosensors have shown promising for POC due to its ease of integration, miniaturization, fast response, cost-effective assay, and conveniently communication with smartphones. The platform presented in this study can be integrated with capillary-driven microfluidics for autonomous and sequentially delivery of analytes. This microfluidics should be precisely designed to control the flow rates in a certain range to have a controlled hydrodynamic washing force for microparticle-labeled immunoassay. To improve the functionality and LOD, further characterization and optimization can be conducted. Previous study showed that the size of nanoparticles does not greatly affect the impedance signal[30]. By considering the ratio of the electrode gap to micro/nanoparticle sizes, optimal biosensing performance can be determined. Furthermore, by incorporating a blood separation membrane on the microfluidic chip and including a communicating chip to interact with a smartphone or a laptop, this device would be an ideal standalone POC platform with high sensitivity and the ability for multiplex diagnostics.

Declaration of interests

The authors declare that they have no known competing financial interests or personal relationships that could have appeared to influence the work reported in this paper.

Acknowledgment

J. Kim acknowledges the financial support of this project from the start-up fund at the University of Utah and from the National Science Foundation Grant NSF-EECS/1509746. A. Khodayari Bavil is partially supported by the Dissertation Completion Fellowship from Texas Tech University.

Figures and Captions

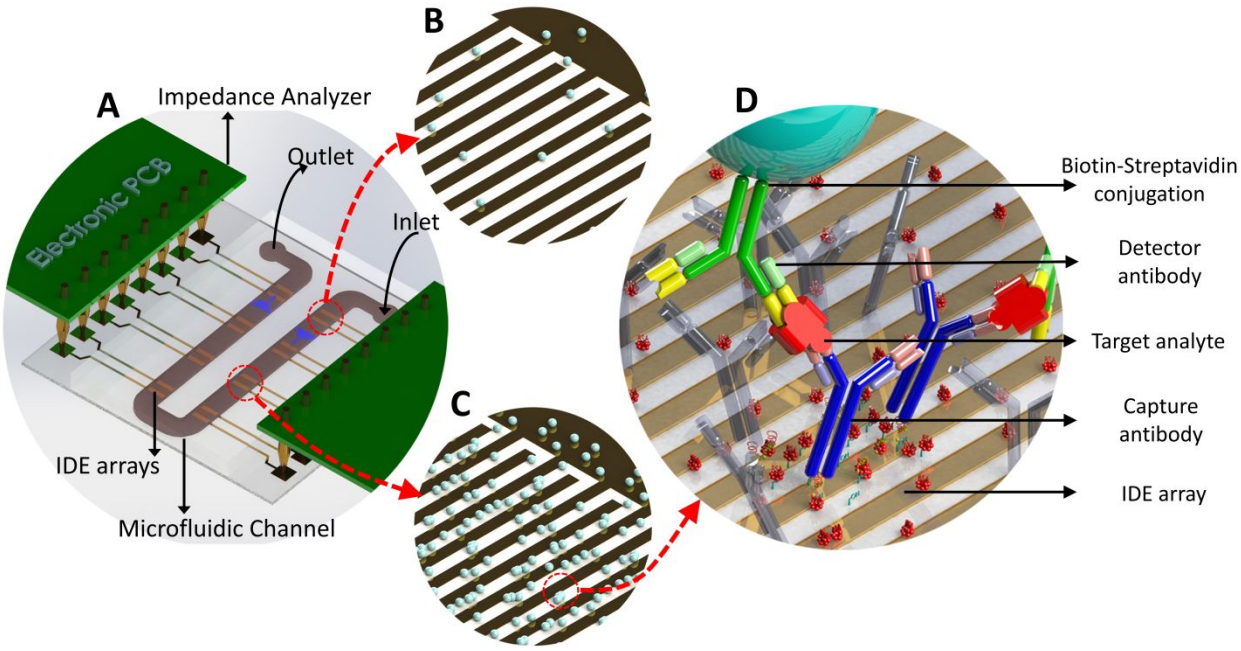

Figure 1.

A schematic diagram of a microfluidic impedance sensor array for microparticle-labeled Immunoassays. (A) Eight interdigitated electrodes (IDEs) integrated with custom-made impedance analyzers and a microfluidic channel, (B-C) Illustration of IDEs for negative and positive controls, and (D) Formation of the full immunocomplex on the IDE.

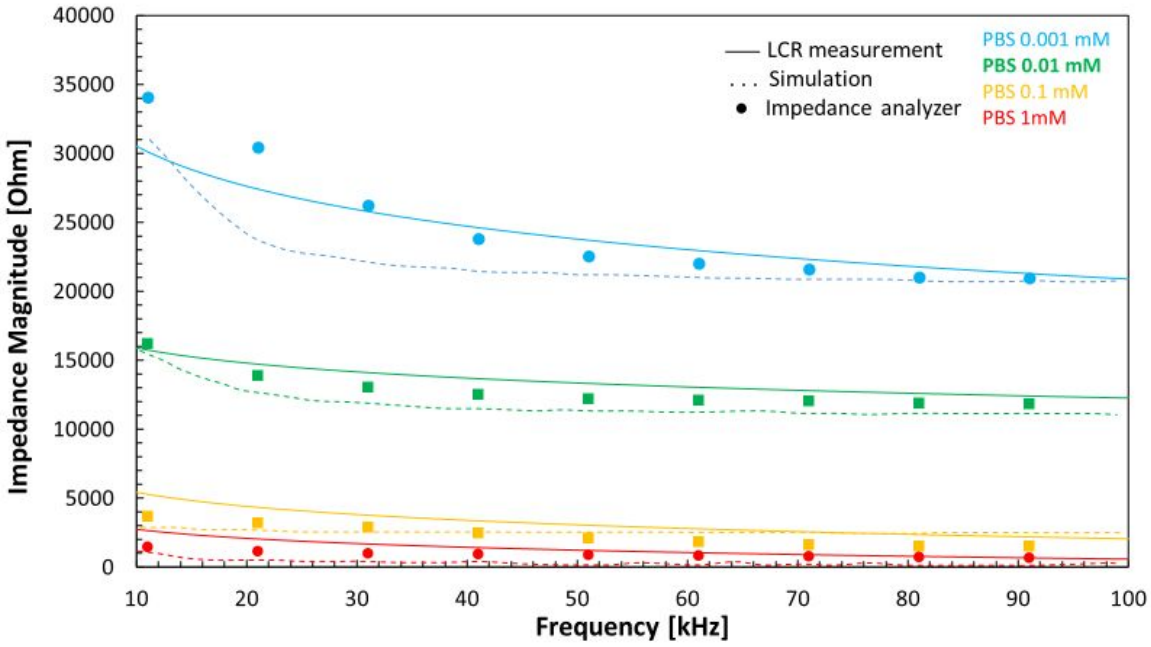

Figure 2.

Different concentrations of phosphate buffer saline (PBS) in deionized water was measured on the IDEs using a commercial LCR meter and impedance analyzer, and calculated form the simulation model. Buffer concentrations of 0.1mM and above show saturations and make it impossible to get impedance variations by immobilization of biomolecules. For PBS 0.01mM less saturation effects were observed, and considering the pH buffer capacity, PBS 0.01mM was selected as a buffer solution during impedance signal measurement.

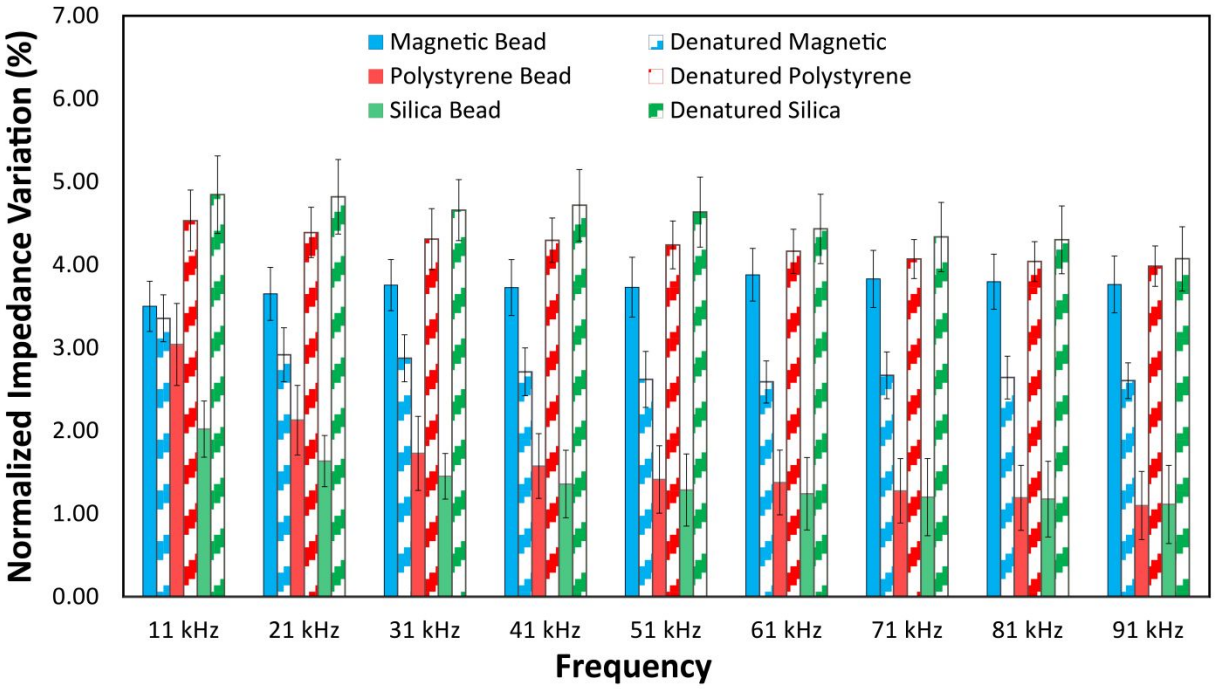

Figure 3.

Three different microparticle types of Magnetic, Polystyrene, and Silica were selected for characterization. All microparticles were at the same size of 2.8μm and the same surface coating of streptavidin for original microparticles. For heat denaturing of microparticles, they have been boiled on a hot plate and then used for impedance measurements. All data are collected for 5% IDE surface coverage.

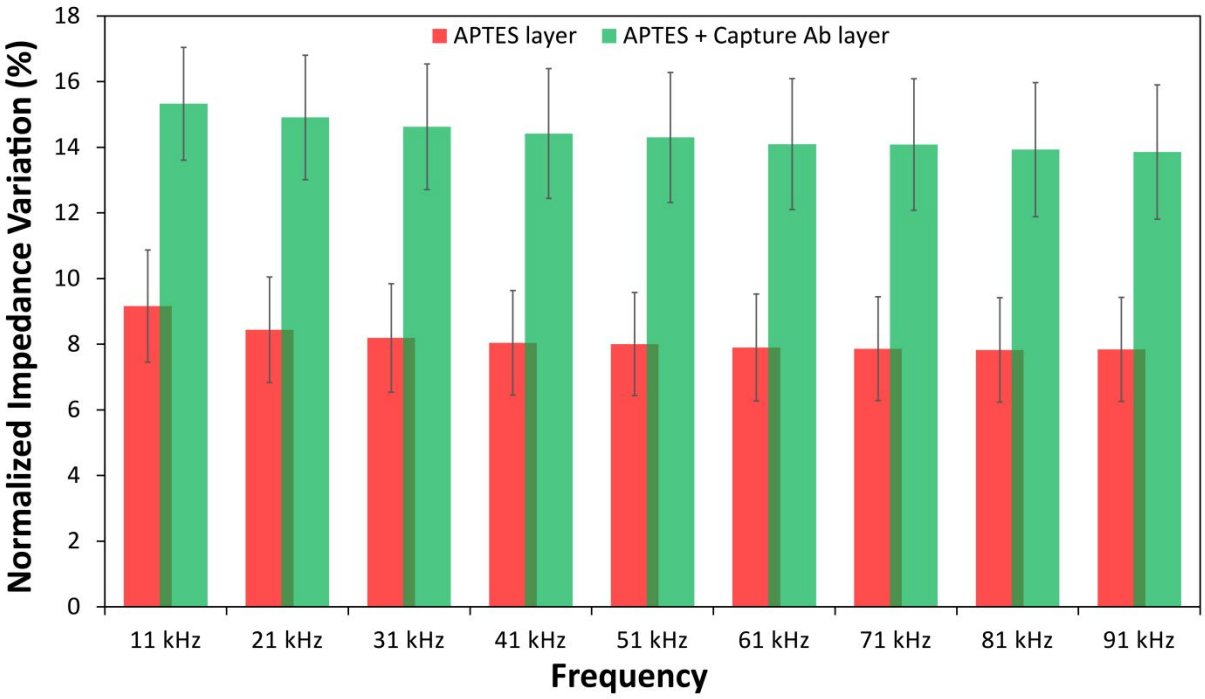

Figure 4.

The normalized impedance variation percentage during surface functionalization. Percent variation of the impedance signals increase with each of APTES and capture antibodies on IDE sensors. These variations slightly decrease with increase of the frequency from 11-91kHz due to the effects of the generated double-layer capacitance.

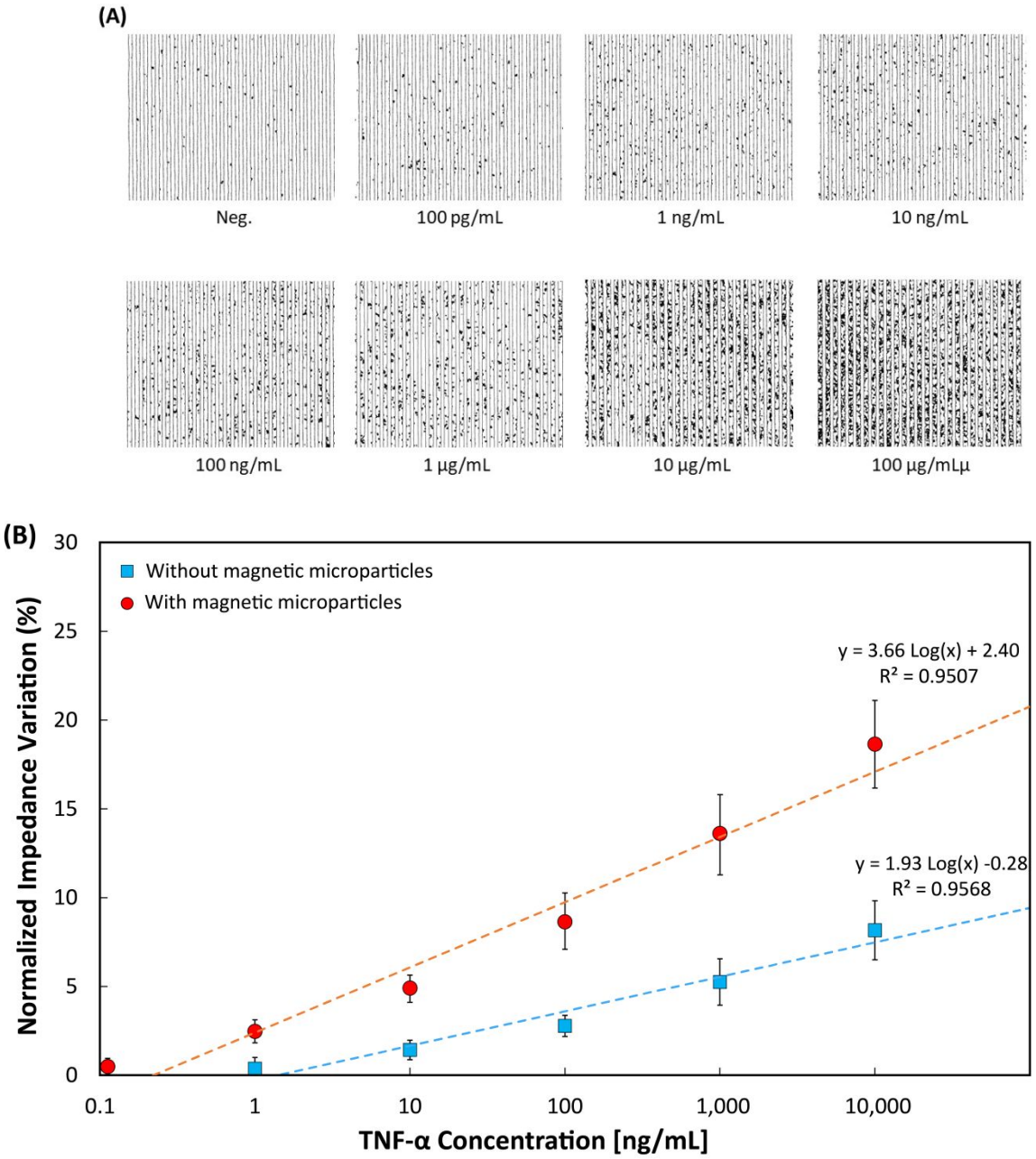

Figure 5.

(A) Magnetic microparticle densities onto the IDE from various target concentrations. (B) Normalized impedance variations comparing capture Ab and various target concentrations (TNF-α) for label-free and sandwich microparticle-labeled at 11 kHz with surface coverage. By the coupling impedance sensor with microparticle-labeled immunoassay format, we were able to detect as low as 83.46 pg/mL of TNF-α. This combination sensing technique enables an order of magnitude of improved sensitivity.

References

1. H. Ma, R. W. Wallbank, R. Chaji, J. Li, Y. Suzuki, C. Jiggins and A. Nathan, *Sci Rep*, 2013, **3**, 2730.
2. R. A. Schramm, M. H. Koslow, D. A. Nelson, M. Larsen and J. Castracane, *Biosensors (Basel)*, 2017, **7**.
3. Y. Liu, D. Zhang, E. C. Alocilja and S. Chakrabartty, *Nanoscale Res Lett*, 2010, **5**, 533-538.
4. A. Lakey, Z. Ali, S. M. Scott, S. Chebil, H. Korri-Youssoufi, S. Hunor, A. Ohlander, M. Kuphal and J. S. Marti, *Biosens Bioelectron*, 2019, **129**, 147-154.
5. J. Tu, R. M. Torrente-Rodríguez, M. Wang and W. Gao, *Advanced Functional Materials*, 2019.
6. S. Ha, M. Diez-Silva, E. Du, S. Kim, J. Han, M. Dao and A. Chandrakasan, Okinawa, Japan, 2012.
7. S. Jin, Z. Ye, Y. Wang and Y. Ying, *Sci Rep*, 2017, **7**, 43175.
8. F. Lisdat and D. Schafer, *Analytical and Bioanalytical Chemistry*, 2008, **391**, 1555-1567.
9. K. V. Singh, D. K. Bhura, G. Nandamuri, A. M. Whited, D. Evans, J. King and R. Solanki, *Langmuir*, 2011, **27**, 13931-13939.
10. P. Van Gerwen, W. Laureyn, W. Laureys, G. Huyberechts, M. O. De Beeck, K. Baert, J. Suls, W. Sansen, P. Jacobs, L. Hermans and R. Mertens, *Sensor Actuat B-Chem*, 1998, **49**, 73-80.
11. V. Dharuman, I. Grunwald, E. Nebling, J. Albers, L. Blohm and R. Hintsche, *Biosensors & Bioelectronics*, 2005, **21**, 645-654.
12. H. Li, X. Liu, L. Li, X. Mu, R. Genov and A. J. Mason, *Sensors (Basel)*, 2016, **17**.
13. K. V. Singh, A. M. Whited, Y. Ragineni, T. W. Barrett, J. King and R. Solanki, *Anal Bioanal Chem*, 2010, **397**, 1493-1502.
14. E. Kostal, S. Kasemann, C. Dincer and S. Partel, *Proceedings*, 2018, **2**.
15. Z. Zou, J. Kai, M. J. Rust, J. Han and C. H. Ahn, *Sensors and Actuators A: Physical*, 2007, **136**, 518-526.
16. S. Hardeman, T. Nelson, D. Beirne, M. DeSilva, P. J. Hesketh, G. J. Maclay and S. M. Gendel, *Sensors and Actuators B: Chemical*, 1995, **24**, 98-102.
17. C. H. Chuang and M. O. Shaikh, in *Point-of-Care Diagnostics - New Progresses and Perspectives*, 2017, pp. 171-201.
18. L. Montelius, J. O. Tegenfeldt and T. G. I. Ling, *J Vac Sci Technol A*, 1995, **13**, 1755-1760.
19. Y. Duan, G. Clark and R. S. C. Cowan, *Proc. SPIE: Smart Structures Devices*, 2001, 498–508.
20. G. B. Kato, Massachusetts Institute of Technology, 2015.
21. A. Santos, *Journal of Analytical & Bioanalytical Techniques*, 2014, **S7**.
22. C. H. Chuang, Y. C. Du, T. F. Wu, C. H. Chen, D. H. Lee, S. M. Chen, T. C. Huang, H. P. Wu and M. O. Shaikh, *Biosens Bioelectron*, 2016, **84**, 126-132.
23. Y. Xu, H. Cai, P. G. He and Y. Z. Fang, *Electroanalysis*, 2004, **16**, 150-155.
24. H. Peng, C. Soeller, M. B. Cannell, G. A. Bowmaker, R. P. Cooney and J. Travas-Sejdic, *Biosens Bioelectron*, 2006, **21**, 1727-1736.
25. Z. Altintas, S. S. Kallempudi and Y. Gurbuz, *Talanta*, 2014, **118**, 270-276.
26. A. K. Yagati, J. Park, J. Kim, H. Ju, K.-A. Chang and S. Cho, *Japanese Journal of Applied Physics*, 2016, **55**.
27. V. Bhalla, S. Carrara, P. Sharma, Y. Nangia and C. Raman Suri, *Sensors and Actuators B: Chemical*, 2012, **161**, 761-768.
28. T. Sun, C. Bernabini and H. Morgan, *Langmuir*, 2010, **26**, 3821-3828.
29. F. Y. Chang, M. K. Chen, M. H. Wang and L. S. Jang, *Journal of Physics D: Applied Physics*, 2016, **49**.
30. S. MacKay, P. Hermansen, D. Wishart and J. Chen, *Sensors (Basel)*, 2015, **15**, 22192-22208.
31. C. H. Yeh, K. F. Su and Y. C. Lin, *Sensor Actuat a-Phys*, 2016, **241**, 203-211.

32. M. A. Ali, P. R. Solanki, S. Srivastava, S. Singh, V. V. Agrawal, R. John and B. D. Malhotra, *ACS Appl Mater Interfaces*, 2015, **7**, 5837-5846.
33. C. M. Pandey, S. Augustine, S. Kumar, S. Kumar, S. Nara, S. Srivastava and B. D. Malhotra, *Biotechnol J*, 2018, **13**.
34. A. Khodayari Bavil and J. Kim, *Analyst*, 2018, **143**, 3335-3342.
35. A. Pierres, A. M. Benoliel and P. Bongrand, *J. Biological Chemistry*, 1995, **270**, 26586-26592.
36. J. Kaur, K. V. Singh, A. H. Schmid, G. C. Varshney, C. R. Suri and M. Raje, *Biosens Bioelectron*, 2004, **20**, 284-293.
37. S. P. Mulvaney, C. L. Cole, M. D. Kniller, M. Malito, C. R. Tamanaha, J. C. Rife, M. W. Stanton and L. J. Whitman, *Biosens. Bioelectron.*, 2007, **23**, 191-200.
38. H. C. Tekin, M. Cornaglia and M. A. M. Gijs, *Lab Chip*, 2013, **13**, 1053-1059.
39. L. Yang, Y. Li and G. F. Erf, *Anal Chem*, 2004, **76**, 1107-1113.
40. S. W. Chen and R. W. Murray, *J Phys Chem B*, 1999, **103**, 9996-10000.
41. A. Oki, Y. Takamura, Y. Ito and Y. Horiike, *Electrophoresis*, 2002, **23**, 2860-2864.
42. K. Skucha, S. Gambini, P. Liu, M. Megens, J. Kim and B. Boser, *J Microelectromech Syst*, 2013, **22**, 1327-1338.
43. K. Skucha, P. Liu, M. Megens, J. Kim and B. Boser, presented in part at the 16th International Solid-State Sensors, Actuators and Microsystems Conference, 2011.
44. P. P. Liu, K. Skucha, Y. Duan, M. Megens, J. Kim, Izyumin, II, S. Gambini and B. Boser, *IEEE J Solid-State Circuits*, 2012, **47**, 1056-1064.
45. J. K. Dhont and K. Kang, *Eur Phys J E Soft Matter*, 2010, **33**, 51-68.
46. R. G. Acres, A. V. Ellis, J. Alvino, C. E. Lenehan, D. A. Khodakov, G. F. Metha and G. G. Andersson, *J Phys Chem C*, 2012, **116**, 6289-6297.
47. C. Berggren, B. Bjarnason and G. Johansson, *Electroanalysis*, 2001, **13**, 173-180.
48. C. Popa, M. G. Netea, P. L. van Riel, J. W. van der Meer and A. F. Stalenhoef, *J Lipid Res*, 2007, **48**, 751-762.
49. J. Abdolalizadeh, J. Majidi Zolbanin, M. Nouri, B. Baradaran, A. Movassaghpour, S. Farajnia and Y. Omidi, *Adv Pharm Bull*, 2013, **3**, 19-23.
50. A. Shrivastava and V. Gupta, *Chronicles of Young Scientists*, 2011, **2**.
51. D. A. Armbruster and T. Pry, *Clin Biochem Rev*, 2008, **29 Suppl 1**, S49-52.
52. K. S. Shin, J. H. Ji, K. S. Hwang, S. C. Jun and J. Y. Kang, *Biosens Bioelectron*, 2016, **85**, 16-24.
53. Y. T. Chen, A. G. Kolhatkar, O. Zenasni, S. Xu and T. R. Lee, *Sensors (Basel)*, 2017, **17**.
54. W. de Jager and G. T. Rijkers, *Methods*, 2006, **38**, 294-303.
55. Y. K. Low, J. Chan, G. V. Soraya, C. Buffet, C. D. Abeyrathne, D. H. Huynh, E. Skafidas, P. Kwan and S. J. Rogerson, *Sensors (Basel)*, 2019, **19**.
56. Y. H. Chuang, Y. T. Chang, K. L. Liu, H. Y. Chang and T. R. Yew, *Biosens Bioelectron*, 2011, **28**, 368-372.